ELSEVIER

Mixing in T-junctions

J. B. W. Kok and S. van der Wal

University of Twente, Enschede, The Netherlands

The transport processes that are involved in the mixing of two gases in a T-junction mixer are investigated. The turbulent flow field is calculated for the T-junction with the k-ε turbulence model by FLOW3D. In the mathematical model the transport of species is described with a mixture fraction variable for the average mass fraction and the variance of the mixture fraction for the temporal fluctuations. The results obtained by numerical simulations are verified in a well-defined experiment. The velocity as well as the concentration field are measured in several types of T-junctions. Comparison of the predicted and measured average concentration fields show good agreement if the Schmidt number for turbulent diffusion is taken as 0.2. Temporal concentration fluctuations are calculated and found to be of equal magnitude as spatial fluctuations. Good mixing is obtained in a T-junction if the branch inlet flow is designed to penetrate to the opposite tube wall in the mixer.

Keywords: turbulent, mixing, mixer, concentration, gas, jet, cross-flow, transport

1. Introduction

Mixing of gases in internal flows occurs in many applications related to the process industry and power generation. A good example is the production of natural gas of a required calorific value. Natural gas from several production wells and nitrogen are mixed to the specified composition. The production gas is sampled, and on the basis of the samples the individual flows are adjusted. In order to minimize delay times in the feedback a mixer is employed.

The application that will be focused on in this paper is the mixing of natural gas and air for a premixed combustor. This can be a gas engine or a gas turbine. In these applications there is a trend to lean premixed combustion in order to reduce the emission of nitric oxides. In a mixer the fuel gas and air are premixed prior to entering the combustor. Low performance of the mixer can lead to spatial and/or temporal fluctuations in the fuel : air ratio. Near the lean blow-out limit this may cause flame instability and increased CO emission. To indicate ways to minimize these concentration fluctuations efficiently, the mixing process is studied in this paper theoretically and experimentally.

The transport processes that are involved in the mixing of two gases in a turbulent flow are investigated in several types of mixers. Attention is focused on a correct prediction of mixing phenomena and on indicating efficient mixing mechanisms. The design of an industrial mixer has to respond to three competitive criteria: (1) small concentration fluctuations at the outlet, (2) a small volume, and (3) a small pressure drop.

In Section 2 the mathematical model is explained that describes the transport processes in the turbulent flow. This model, which is incorporated in the computational fluid dynamics code FLOW3D, is used to predict the mixing performance of T-junctions under a range of conditions. In order to verify these predictions, the flow field and concentration in the mixer were measured in an experiment. The experimental set-up is discussed in Section 3. The geometry and the grid used to simulate the tested mixer with FLOW3D are shown in Section 4. The measured and predicted velocity field in the mixer are discussed in Section 5. The results on the performance of the tested mixers are described in Section 6. In Section 7 the measured and predicted concentration fields at the mixer outlet are analyzed. Using the simulations, the mechanism that leads to mixing in a T-junction is investigated. Conclusions regarding mixing mechanisms and their modelling, with a view to design and prediction of performance, are drawn in Section 8.

2. Modeling transport and mixing of species in a turbulent flow

In order to describe the turbulent mixing phenomena and to predict mixing performances, the mass transport in an isothermal incompressible steady three-dimensional flow is modelled mathematically. The starting point is the set of equations describing the instantaneous velocities and mass fractions on the basis of conservation of mass, momentum, and species. When applied to turbulent flow, solutions can

Address reprint requests to Dr. Kok at the Department of Mechanical Engineering, University of Twente, P. O. Box 217, 7500 AE Enschede, The Netherlands.

Received 14 July 1993; revised 16 May 1994; accepted 8 June 1994

655 Avenue of the Americas, New York, NY 10010

0307-904X/96/$15.00
SSDI 0307-904X(95)00151-4

be found for the averaged properties if the equations are closed by turbulence modelling. In this section the turbulence model used for the T-junction for momentum and mass transport will be explained.

In the literature[1-3] the conservation equations in cartesian coordinates x_i, with flow velocity components u_i, are usually written as

$$\frac{\partial}{\partial t}(\rho\phi) + \frac{\partial}{\partial x_i}(\rho\phi u_i) = \frac{\partial}{\partial x_i}\left(\Gamma_\phi \frac{\partial \phi}{\partial x_i}\right) + S_\phi \quad (1)$$

In equation (1), ρ is the fluid density, ϕ the conserved variable, Γ_ϕ a diffusion coefficient, and S_ϕ a source term. In equation (1) (and thereafter) use is made of the Einstein convention of summation over repeated indices. The conservation equation of mass is obtained by substituting $\phi = 1$ into equation (1). Since mixing phenomena in isothermal steady flows at low Mach numbers are considered, the density can be assumed constant and equation (1) reduces to

$$\frac{\partial u_i}{\partial x_i} = 0 \quad (2)$$

The momentum equations are obtained by substituting $\phi = u_i$ and $S_\phi = -\partial P/\partial x_i$ in equation (1)

$$\frac{\partial}{\partial x_i}(\rho u_j u_i) = \frac{\partial}{\partial x_i}\left[\mu\left(\frac{\partial u_j}{\partial x_i} + \frac{\partial u_i}{\partial x_j}\right)\right] - \frac{\partial P}{\partial x_i} \quad (3)$$

Here P is the pressure and μ is the dynamic viscosity of the fluid. In equation (3) the flow was assumed steady and gravity is neglected. In this research the latter was justifiable since the fluid was a mixture of oxygen and nitrogen. Their molar masses are 32 and 28 kg/mol, respectively. Hence buoyancy effects are not likely to occur on a timescale of seconds. Because the residence time of the flow in the T-junction will be less than 1 sec, gravity was neglected in the simulations.

The equation describing transport of an inert species A with mass fraction y_A ($y_A = \rho_A/\rho$) is obtained by taking $\phi = y_A$ and the molecular diffusion coefficient D, $\Gamma_\phi = \rho D$ in equation (1), yielding

$$\frac{\partial}{\partial x_i}(\rho y_A u_i) = \frac{\partial}{\partial x_i}\left(\rho D \frac{\partial y_A}{\partial x_i}\right) \quad (4)$$

In this research the mixing of two species (two inlets) is considered. One inlet flow consists of air and the other of pure nitrogen. Hence if for y_A the oxygen mass fraction (representative for the air concentration) is taken, the mass fraction y_B of inert species is found by the fact that in a binary mixture $y_A + y_B = 1$.

The above equations describe the instantaneous flow variables. In a turbulent flow the velocities and mass fraction will, however, fluctuate in time. In order to calculate and analyze the flow field, the equations are solved for the time average values and the intensities of the fluctuations. As suggested by Sir Osborne Reynolds, the instantaneous variables are decomposed into a time mean averaged over a large time scale T, and a fluctuating part:

$$\phi = \bar{\phi} + \phi' \qquad \text{with } \bar{\phi} = \frac{1}{T}\int_0^T \phi(t+\tau)\,d\tau \quad (5)$$

Equation (5) is substituted into equations (2)–(4). Subsequently they are time averaged in order to obtain equations for the time mean of the flow variables. This leads to the following equations for mass, momentum, and species, respectively:

$$\frac{\partial \bar{u}_i}{\partial x_i} = 0 \quad (6)$$

$$\bar{u}_i \frac{\partial}{\partial x_i}(\rho \bar{u}_j) = \frac{\partial}{\partial x_i}\left[\mu\left(\frac{\partial \bar{u}_j}{\partial x_i} + \frac{\partial \bar{u}_i}{\partial x_j}\right)\right] - \frac{\partial \bar{P}}{\partial x_j} - \frac{\partial}{\partial x_i}(\rho \overline{u_j' u_i'}) \quad (7)$$

$$\frac{\partial}{\partial x_i}(\rho \bar{y}_A \bar{u}_i) = \frac{\partial}{\partial x_i}\left(\rho D \frac{\partial \bar{y}_A}{\partial x_i}\right) - \frac{\partial}{\partial x_i}(\rho \overline{u_i' y_A'}) \quad (8)$$

Equations (7) and (8), which describe the mean flow variables, each have a term on the right-hand side that reflects the effect of the averaged turbulent fluctuations. These two terms, the turbulent stress and the turbulent mass transport, have to be closed by turbulent modelling. Boussinesq suggested a straightforward way to model these turbulent terms. He introduced the "eddy viscosity hypothesis" which assumes an expression of the turbulent terms similar to the corresponding laminar terms but with an adapted turbulent viscosity[3]:

$$-\rho \overline{u_j' u_i'} = \mu_t\left(\frac{\partial \bar{u}_j}{\partial x_i} + \frac{\partial \bar{u}_i}{\partial x_j}\right) - \frac{2}{3}\left(k + \mu_t \frac{\partial \bar{u}_j}{\partial x_i}\right)\delta_{ij} \quad (9)$$

and similarly

$$-\rho \overline{u_i' y_A'} = \frac{\mu_t}{Sc_t}\frac{\partial \bar{y}_A}{\partial x_i} \quad (10)$$

with turbulent kinetic energy $k = (1/2)\overline{u_i' u_i'}$, δ is the kronecker delta, Sc_t is the turbulent Schmidt number, and μ_t is the turbulent viscosity.

The terms are closed by taking an expression for the turbulent viscosity μ_t. If the turbulent flow field is more or less isotropic, equations (9) and (10) can, with satisfactory results, be closed by a simple isotropic expression:

$$\mu_t = C_\mu \rho \frac{k^2}{\varepsilon} \quad (11)$$

Here ε is the rate of dissipation of turbulent kinetic energy. C_μ is a fitting constant that is usually taken equal to 0.09. The variables k and ε are determined by two additional transport equations[4]:

$$\bar{u}_i \frac{\partial k}{\partial x_i} = -\frac{\partial}{\partial x_i}\left(\frac{\mu_t}{\sigma_k}\frac{\partial k}{\partial x_i}\right) + P - \varepsilon \quad (12)$$

$$\bar{u}_i \frac{\partial \varepsilon}{\partial x_i} = -\frac{\partial}{\partial x_i}\left(\frac{\mu_t}{\sigma_\varepsilon}\frac{\partial \varepsilon}{\partial x_i}\right) + \frac{\varepsilon}{k}(C_1 P - C_2 \varepsilon) \quad (13)$$

with production of k

$$P = -\overline{u_i' u_i'} \frac{\partial \bar{u}_i}{\partial x_j} \tag{14}$$

σ_k, σ_ε, C_1, and C_2 are empirical constants. The values recommended by Launder and Spalding were used here.

2.1 Modelling constants

The Boussinesq (gradient hypothesis) model assumes that the turbulent transport mechanism of momentum and scalar quantities (species, heat) by the turbulent eddies can be described analogous to laminar transport but with a different magnitude of the diffusion coefficient. This is shown by equations (9–11). In general the corresponding turbulent diffusion coefficient will depend on the character of the turbulent flow field. Also the turbulent transport of a vector variable, like momentum, and of a scalar variable, like heat or a species, is not necessarily described with one diffusion coefficient. The ratio of the momentum to the scalar-diffusion coefficient is given by the turbulent Schmidt number Sc_t, where $0.1 < Sc_t < 1.0$. The choice of the Schmidt number will be discussed below.

The turbulent diffusion of momentum is determined by the constant C_μ. In the literature the global value of C_μ is usually taken as 0.09. The value of the Schmidt number varies, however, with the flow geometry. In developed tube flow, turbulent scalar diffusion is relatively slow, and for example in the book by Bird et al.[1] (pp. 379, 629) $Sc_t = 0.9$ is suggested. Hence in this case turbulent diffusion coefficients of momentum and species (or heat) are of similar magnitude.

Bird et al.[1] mention a value $Sc_t = 0.5$ for an axisymmetric jet in an otherwise stagnant flow. Hence the jet induces much faster turbulent mixing of species compared with mixing of momentum. According to Patankar[5] (p. 173) such a turbulent jet issuing from a circular orifice can be analyzed as a two-dimensional parabolic flow. It is well known in the literature that the k-ε turbulence model cannot describe the turbulent diffusion of momentum in such an axisymmetric jet emerging in a stagnant flow. The turbulent diffusion of momentum is for this type of jet overpredicted by 30% if the k-ε model is used.[6]

The situation investigated in this paper is different however. A turbulent jet issuing from a circular orifice that is deflected by a stream normal to its axis induces a three-dimensional elliptic flow. An impression of the flow pattern is given in Figure 9.10 in Patankar.[5] Patankar et al.[7] solved numerically the three-dimensional flow field of the deflected jet on the basis of the k-ε model of turbulence. As their Figures 9.11 and 9.12, in Patankar[5] show, they find good agreement between numerical prediction and experiment.

In our research the jet is not deflected by an infinitely large cross-flow but by a cross-flow in a tube. Basically the flow field is, however, similar to that in Patankar et al.,[5,7] and therefore good results for the prediction of flow field and turbulent mixing are expected with the k-ε model of turbulence. Since Patankar et al.[5,7] also used $C_\mu = 0.09$ this will most probably predict turbulent mixing of momentum correctly. The only remaining unknown parameter is the Schmidt number Sc_t. Because the flow field is different in character from a jet in stagnant flow, it is not likely that $Sc_t = 0.5$. For that reason the possibility will be investigated in this paper of a universal value of the Schmidt number for the deflected jet flow. This will have to give good numerical prediction of turbulent mixing of mass for all flows in the T-junction that we considered in the experiments.

The mean mass fraction of oxygen y_A is described by equation (8), (10), and (11). In FLOW3D it is possible to solve this equation. As stated earlier for turbulent mixing, not only the mean mass fraction but also the amplitude of the temporal fluctuations is of interest. It is possible to calculate this as well with FLOW3D by making use of the built-in mixed = burnt combustion model. In this model a fluid A (fuel) is mixed with a fluid B (oxidizer) and reacts in a stoichiometric ratio i to a product. The mass fraction y_A of fluid A with respect to the mass fraction y_B of fluid B is denoted with the mixture fraction f. In a flow that has two inlet streams, the mixture fraction f is defined as:

$$f = \frac{\chi - \chi_1}{\chi_2 - \chi_1}$$

$$\begin{aligned} \text{with} \quad & \text{inlet 1: } y_A = y_{A1},\ y_B = y_{B1} \\ & \text{inlet 2: } y_A = y_{A2},\ y_B = y_{B2} \\ & \chi = y_A - y_B/i \\ & \chi_1 = y_{A1} - y_{B1}/i \\ & \chi_2 = y_{A2} - y_{B2}/i \end{aligned} \tag{15}$$

Thanks to its definition f is a conserved variable and varies in the range 0–1. In a binary mixture, without reaction between the species, expression (15) for f can be simplified to

$$f = \frac{y_A - y_{A1}}{y_{A2} - y_{A1}} \tag{16}$$

Hence in the case of pure mixing, f is independent of the reaction constant i. If we take for inlet 1 air flow and for inlet 2 a flow of nitrogen (see the next section), $y_{A1} \approx 0.2$ and $y_{A2} = 0$. Thanks to the latter inlet condition, f is a dimensionless expression for the local deviation of y_A from the value at inlet 1:

$$f = (y_{A1} - y_A)/y_{A1} \tag{17}$$

The temporal variance of f, and hence y_A, is denoted with $g = \overline{f'f'}$. Spalding[8] formulated a modelled transport equation for g (f is a conserved variable with transport equation like [8]):

$$\frac{\partial}{\partial x_i}(\rho g \bar{u}_i) = \frac{\partial}{\partial x_i}\left[\left(\rho D + \frac{\mu_t}{Sc}\right)\frac{\partial g}{\partial x_i}\right] + C_{g1}\frac{\mu_t}{Sc}\left(\frac{\partial f}{\partial x_i}\right)^2 - C_{g2}\rho\frac{\varepsilon}{k}g \tag{18}$$

with $g = \overline{f'f'}$

The mixed = burnt combustion model in FLOW3D solves transport equations for f and g.[9] This model can be used to predict temporal fluctuations in isothermal mixing

as well. In our nonreacting mixing flow we can set the heat of reaction to zero. Because we have a binary mixture, y_A as a function of (r, θ, x) is calculated from the mixture fraction f with equation (17). The variable g gives the time variance of y_A as a function of (r, θ, x). This way by using the mixed = burnt combustion model for an isothermal mixing flow the spatial gradient of the mean oxygen mass fraction and the variance of the temporal fluctuations can be calculated.

The value recommended by Spalding[8] was taken for the empirical constants C_{g2}, C_{g1} in equation (18). This equation clearly shows that temporal fluctuations are driven by a source term proportional to the square of the gradient in f. Hence large gradients in the concentration (hence in f) will lead to large temporal fluctuations in the concentration as well. Temporal fluctuations are damped by a term proportional to the ratio ε/k. The balance between these two terms on the right-hand side of equation (18) will determine the amplitude of the temporal fluctuations.

2.2 Literature on turbulent scalar transport and jets in a cross-flow

The turbulent jet in a cross-flow has important engineering applications; therefore there can be found an impressive number of references in the literature. A large category of applications is the row of jets in the dilution zone of a gas turbine combustion chamber. Cold air from the jets is mixed with hot exhaust gas to a mixture temperature acceptable for the turbine blades. In this field a lot of computational and experimental research is performed at the NASA/Lewis Research Center, Cleveland,[10,17] and at United Technologies.[18]

Claus and Vanka[10,11] investigated the use of multigrid techniques to obtain grid-independent calculations. Demuren[12-15] applied multigrid techniques and the k-ε as well as a Reynolds stress turbulence model to a jet in a cross-flow. Both turbulence models predict very well the mean flow properties. The Reynolds stress model gives superior prediction of the turbulent stresses compared with measurements. Unfortunately turbulent scalar transport is not investigated. Demuren gives an extensive review on modelling approaches.[12]

Also at the Lewis Research Center, Kim and Benson improved the prediction of turbulent diffusion of momentum in a jet in a cross-flow by taking into account different time scales for turbulent momentum transport and the rate of dissipation.[16] The transport of mass and momentum is determined by the large eddies and the dissipation rate by the fine-scale eddies. In fact this leads to an eddy viscosity model with a local variable C_μ. Two additional transport equations are introduced.

Holdeman[17] summarizes experimental and computational results on the mixing of (rows of) jets in a confined cross-flow. In this extensive review more than 160 references are cited since 1970. Important for the present work is that he concludes that there is a relation between the temperature distribution at the exit, the momentum flux ratio of jet and cross-flow, and orifice spacing.

Measurements and simulations of (multiple) jets impinging through a cross-flow are performed by Barata et al. at the Instituto Superior Tecnico, Lisboa,[19,20] and at Imperial College, London.[21,22] The latter paper is often used as a reference by other authors for calculations of a jet in an unbounded cross-flow.

Andreopoulos and Rodi[23] present detailed measurements of the mean flow field and the turbulent stresses of a jet in an unconfined cross-flow. They analyze their measurements with a view to application of an eddy-viscosity model in numerical calculations. They conclude that in general this can be applied for the production of turbulent kinetic energy and two of the shear stresses. The prediction of the production of the axial-tangential turbulent shear stress by the eddy viscosity model is in certain regions troublesome. Unfortunately the turbulent scalar transport fluxes were not measured.

Ferrell and Lilley[24] conducted experiments of the flow-field of a deflected jet in a confined (nonswirling) cylindrical cross-flow. They found that the jet penetration was reduced from that of comparable velocity ratio infinite cross-flow cases. Their measurements confirmed that the deflected jet is symmetrical about the vertical plane passing through the cross-flow axis.

It can be concluded that despite the inaccuracy in one of the turbulent shear stresses, it is possible to calculate a correct mean flow field with the eddy viscosity model. It is not clear from the literature if it is possible or not to calculate a mean species concentration field with this model.

The prediction of turbulent scalar diffusion can be improved by calculating the local Schmidt number from first principles instead of taking a global empirical value. A good review of advanced two-equation models of turbulent scalar diffusion, applied to general flows, can be found in Horiuti.[25] In these advanced models the velocity field is calculated with the conventional k-ε model. Subsequently the scalar transport is calculated with an equation for the mean mass fraction like equation (8) and two additional equations for the fluctuation of the mass fraction (here variable g, equation [18]) and the rate of dissipation of this fluctuation. This means that the modelling terms in equation (18) are replaced in this approach by terms with an additional variable and associated transport equation. A comparable approach, applied to a jet in a cross-flow, was taken by Kim and Benson.[16] Even more sophisticated models, taking into account anisotropy, are described in Horiuti[25] as well. Leboeuf et al.[26] followed a different approach. They derived an integral formulation for the trajectory of a single jet or multiple jets in an unbounded cross-flow.

For a start, as we will see in Sections 5 to 7, the relatively simple f, g model with suitable Schmidt number already can provide the designer with useful information on the T-junction flow.

3. Experimental set-up

Two experimental set-ups were used. One set-up was used to measure the concentration profile of the mixture at the

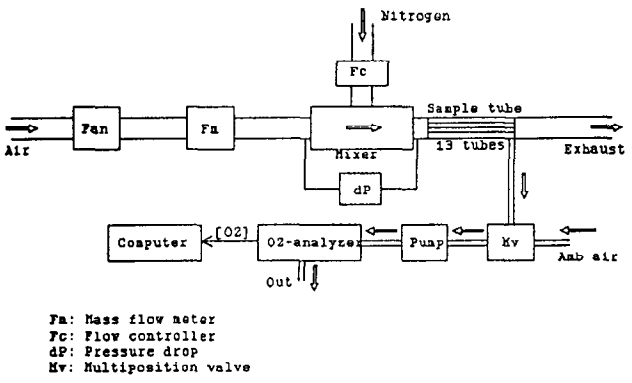

Figure 1. Experimental set-up for the concentration measurements.

mixer outlet. In order to use these measurements for a verification of the numerical simulations, both the concentration field and the velocity field have to be determined. Therefore a second experimental set-up was used to measure the axial and radial velocity in the axial-radial symmetry plane of the mixer.

The performance of the mixer when mixing nitrogen and air was determined for several flow ratios and diameters of the branch inlet of the T-junction. The experimental set-up used was situated at the N.V. Nederlandse Gasunie Laboratory in Groningen (NL) and is sketched in *Figure 1*. Air is blown by a fan through a mass flow meter to the main inlet of the T-mixer. The branch inlet is fed with a nitrogen flow by a flow controller equipped with an electronic mass flow meter as well. The average oxygen concentration (representative for the air mass fraction) was measured at 13 positions in the outlet cross-section of the mixer. This was done by switching a 14 position sample valve (Valco) subsequently to one of the 13 sample probes in the mixer outlet and the ambient. The oxygen concentration was determined by the analyzer and averaged over 12 sec.

In order to verify the dependence of the flow through the mixer on the flow ratio of the two inlet streams and the branch diameter, the flow pattern was investigated experimentally. The velocity field was determined in a representative axial cross-section of the mixer with the use of laser doppler velocimetry. In a gas flow laser doppler velocity measurements are difficult to perform. For this reason in this experiment the fluid used was water instead of an air/nitrogen mixture. The Reynolds number of water flow in the outlet, however was identical to that of the air/nitrogen flow in which the concentration measurements were performed. A schematic view of the experimental set-up is given in *Figure 2*. This set-up was located in the laboratory of the University of Twente. In the experiment water is pumped by a 1.5 kW centrifugal pump (*Figure 2*#7), from an open settling tank (#5) through a flow meter (#4) to a tube system that consists of three parts. These are an inlet (#6) and outlet pipe of diameter 0.1 m coupled with a measurement tube section (#2, the mixer) of length 0.5 m. The outlet tube returns the flow to the settling tank. The inlet section is equipped with a 0.3 m long honeycomb flow straightener to provide the mixer inlet with a well-defined uniform inlet flow profile with a low turbulence intensity. A second tube system, diameter 32 mm, connects the pump via a rotameter (flow meter #8) to the branch inlet. The desired flows and flow ratio are obtained by adjusting valves in the tubes from the pump and a shunt flow over the pump.

In order to suppress density gradients in the water due to a temperature rise by the dissipated pump power (1.5 kW), the settling tank was cooled. During the measurements the difference between ambient and water was kept smaller than 0.2°C.

The axial and radial velocity profiles in the mixer were measured simultaneously with a two-component laser doppler velocity meter.[27,28] This is a forward scattering system (*Figure 2*, #3) with two signal sensors at the other side of the tube (#9). The mixer was placed in a square water-filled perspex optical box (#1) to eliminate the effect of refraction at the cylindrical tube wall. At each measurement location the signal representing the instantaneous velocities was sampled 2,000 times in a period of 60 sec. Using these samples, the average velocity was calculated. The velocity field was measured in the axial-radial symmetry plane of the T-mixer.

4. Geometry

The following mixer geometries were investigated in the experiments: A T-junction with branch diameter variable to 10, 19, or 26 mm, a T-junction with a branch inlet of 100 mm, a venturi mixer with radial jet inlet at the throat, and a swirler in an expanding tube. All mixers had a main inlet and outer diameter of 100 mm. With the computational fluid dynamics package FLOW3D the T-mixers were simulated. Here we will focus on the results with the 10–26 mm branch T-junction. Results of the other experiments are helpful.[28] In *Figure 3* the geometry of the mixer is given. The geometry of the 100 mm branch T-junction is given in *Figure 4*. Flows are from left to right through the mixer.

The geometry of the mixer in *Figure 3* can be described relatively simply with a mesh of grid points. The

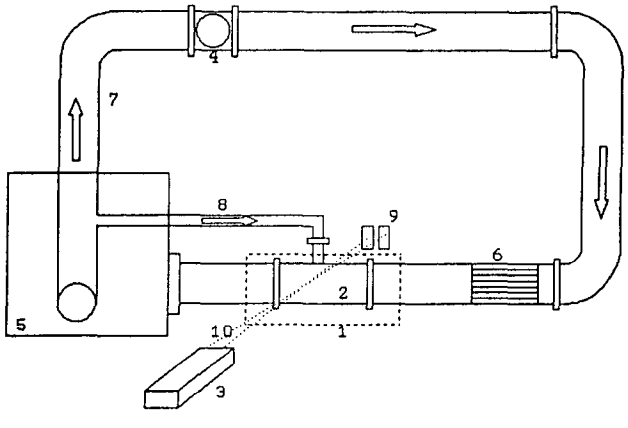

Figure 2. Experimental set-up for the laser doppler velocity measurements.

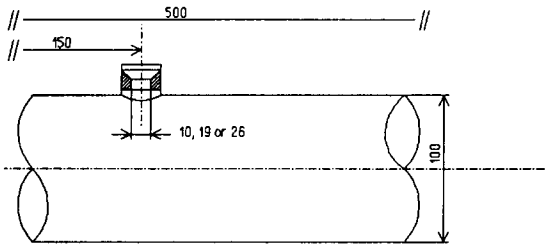

Figure 3. T-junction mixer with branch inlet 10–26 mm.

flow is three-dimensional, but the flow at the branch inlet can be assumed to be uniform and purely vertical due to the small inlet diameter and high inlet velocity. For that reason a mesh was generated in FLOW3D version 2.4 that was uniform and cartesian. This is depicted in *Figure 5* with an axial and a radial cross-section. The number of nodes in the axial, horizontal, and vertical directions was, respectively, 86, 12, and 26. The branch was modelled with, respectively, 12, 6, and 2 nodes. Only half the cross-section was described because there is an axial-radial symmetry plane in the branch inlet and the mixer.

The boundary conditions for this geometry and the next were as follows. The three velocity components, the turbulent kinetic energy, and its rate of dissipation were prescribed at the run and branch inlet. The plane through the centerline of the branch and the run inlet was a plane of symmetry.

With this mesh about 1,500 iterations were necessary for FLOW3D to obtain a converged solution with small residuals. This took about 10 hr of CPU time on a Convex C240 main frame computer. In order to minimize numerical diffusion, the QUICK scheme was used. As a check for some cases the power law scheme was used and/or the number of grid cells decreased by 50%. This did not have a relevant effect on the calculation results.

The geometry of the mixer in *Figure 4* is much more difficult to describe with a mesh of grid points. This is because the 100 mm branch inlet has a large diameter with large velocities. The assumptions of parallel stream lines and uniform flow in the branch inlet will not be valid here. In order to take account of this a cartesian mesh containing six blocks was generated in FLOW3D version 3.1. This is depicted in *Figure 6*. The number of nodes in the axial, horizontal, and vertical directions were respectively, 85, 10, and 20. The total number of nodes in the branch inlet

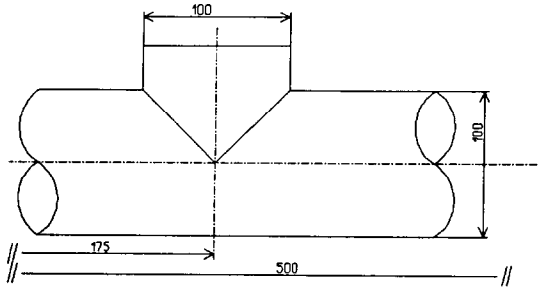

Figure 4. T-junction mixer with branch inlet 100 mm.

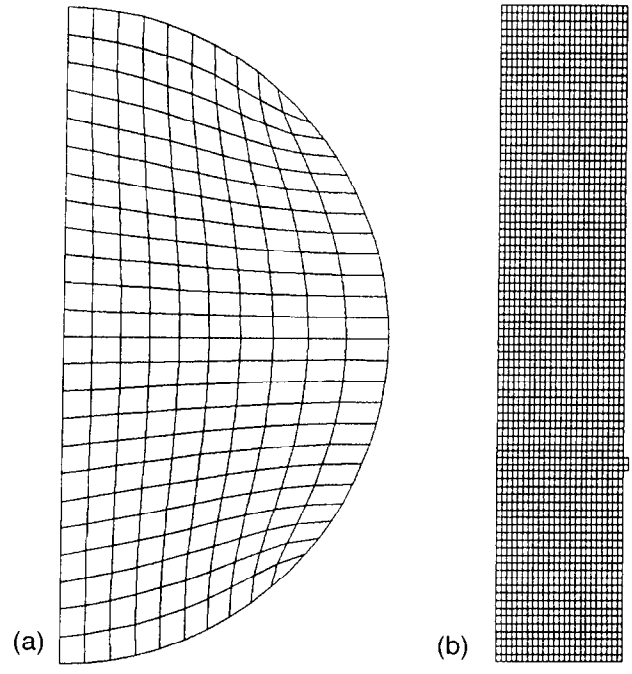

Figure 5. Computational mesh employed for the T-junction with 10–26 mm branch inlet. (a) Radial cross-section (b) Axial cross-section.

block was 200. With this mesh and the QUICK scheme, FLOW3D needed about 2,000 iterations to calculate a converged solution. This took 15 hr of CPU time on an HP 9000/710 workstation. For the results of the calculations with this mesh, refer to Van der Wal.[28]

5. Results: Velocity field

With the experimental set-up at the University of Twente as described in Section 3, a measurement program was performed in which the flow field was determined in the axial-radial symmetry plane. For each branch diameter, 10, 19, and 26 mm, the ratio of the flow through the branch to the flow through the run was varied as 0.05, 0.1, 0.13, and 0.2. The Reynolds number at the outlet was kept constant to 10,000. The goal of these measurements was to verify

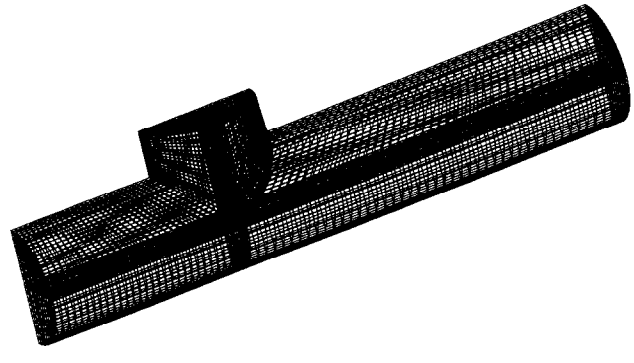

Figure 6. Computational mesh employed for the T-junction with 100 mm branch inlet.

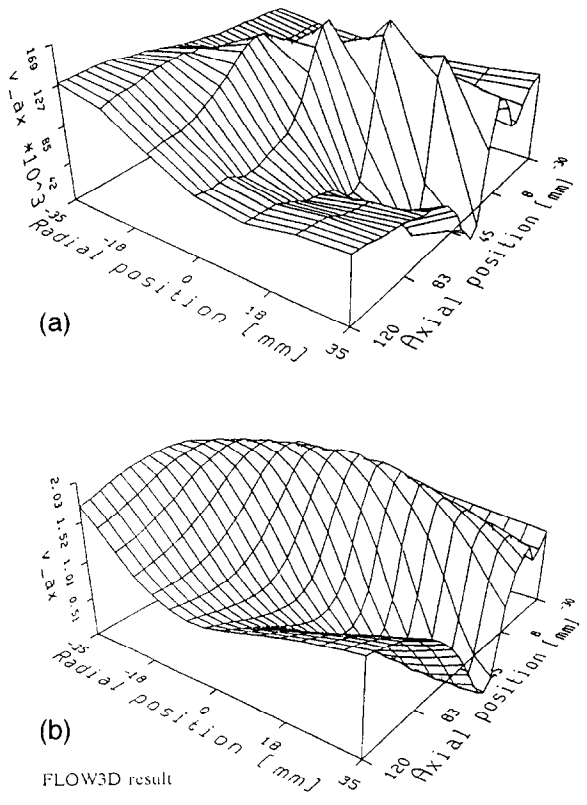

Figure 7. Axial velocity field with a 26 mm branch inlet and mixture ratio 0.2. (a) Measured. (b) FLOW3D prediction.

the numerical simulations with FLOW3D that were made for the flow ratios and branch diameters mentioned above. The axial and radial velocity fields of simulations and measurements were compared.

A typical result is shown in *Figure 7*. The branch inlet diameter was 26 mm, and the branch to run inlet flow ratio was 0.2. Here the axial velocity field measured (*Figure #7a*) and predicted by simulation (*Figure #7b*) in the axial radial symmetry plane are depicted. In *Figure 7a* we see that at the run inlet, axial position -30 mm, the axial velocity field is almost uniform. At the branch inlet, axial position 0 mm, the axial velocity increases due to the inflow. Immediately downstream of the branch inlet the axial velocity decreases strongly since here is the wake of the inflowing jet. There is a small region of reversed flow near axial position 45 mm. Downstream of the branch position the axial velocity maximum moves toward the opposite tube wall.

The axial flow field predicted by FLOW3D compares very well with these measurements as can be seen in *Figure 7b*. Even small details can be seen both in *Figures 7a* and *7b*, for example not only the region of flow reversal downstream of the jet but also the small decrease in velocity upstream of the jet at radial position 35 mm. It should be remembered that the simulations were performed with the air/nitrogen mixture as a medium and the velocity measurements in water. The kinematic viscosities of these fluids are, respectively, $\nu = 1.5104.10^{-5}$ m^2/sec and $\nu = 1.00378.10^{-6}$ m^2/sec. To obtain identical Reynolds numbers the water velocities at the mixer inlet were adjusted accordingly.

The radial velocity field associated with the axial velocities in *Figure 7* measured (a) and simulated (b), is shown in *Figure 8*. Both simulations and measurements show that the vertical jet penetrates to a radius of approximately -20 mm. The axial deflection at that point is predicted and measured as about 80 mm from the branch inlet centerline. In the wake of the jet, the radial velocity has a local minimum.

The effect of the Reynolds number on the velocity field was verified by a set of experiments at $Re = 20{,}000$ and 2,000. The experiments did not show a change of the flow field by increasing the Reynolds number to 20,000. Decreasing the Reynolds number to 2,000, and thus obtaining a laminar flow field, did show some flow field changes.

As a conclusion it can be stated that the axial and radial velocity field of the T-junction as predicted by FLOW3D calculations compare very well with the measured velocity fields. *Figures 7* and *8* give a good illustration of this result. The complete data are available elsewhere.[28]

6. Results: The concentration field

With the experimental set-up at the laboratory of the Nederlandse Gasunie as described in Section 3, the distribution of the oxygen concentration was determined in the cross-section of the mixer outlet. At 3 radii of 4 lines, at

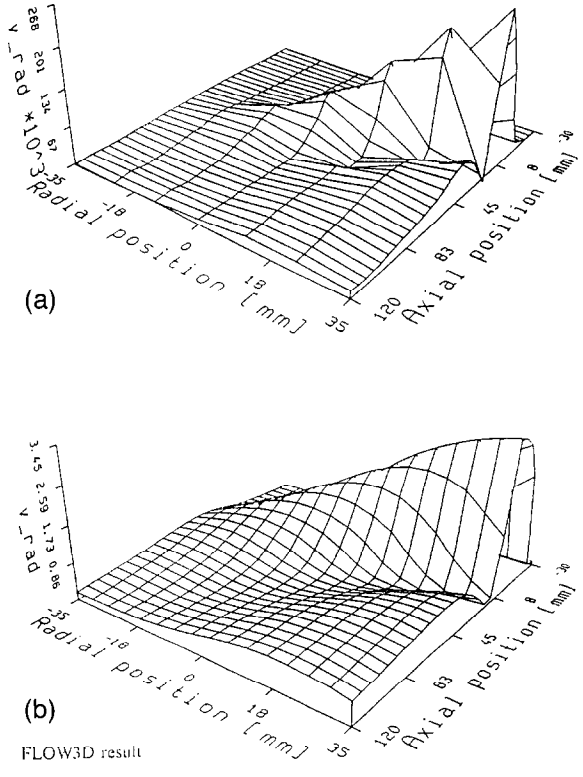

Figure 8. Radial velocity field with a 26 mm branch inlet and mixture ratio 0.2. (a) Measured. (b) FLOW3D prediction.

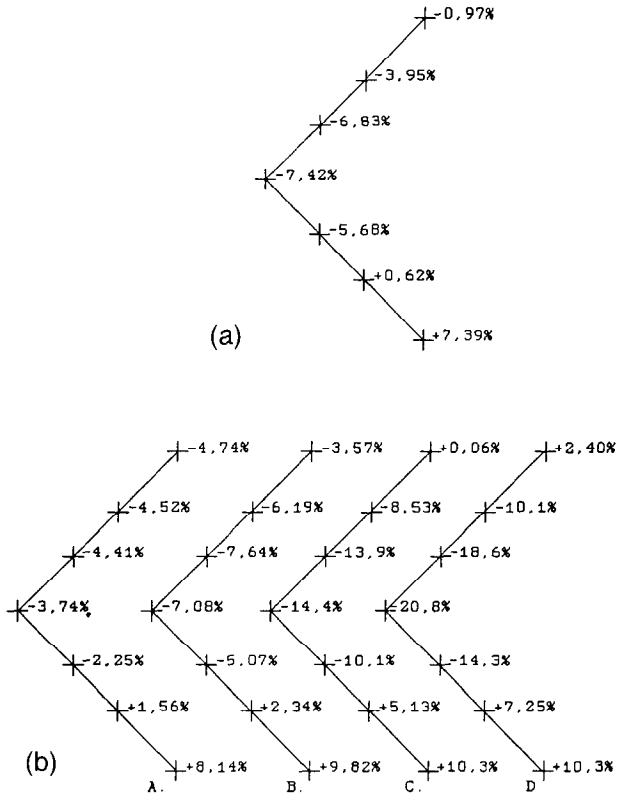

Figure 9. Relative deviation of the oxygen concentration from the average. (a) Measured. (b) FLOW3D prediction with Sc = A:0.1, B:0.2, C:0.5, D:0.9.

90° angles, $3 \times 4 = 12$ points, the oxygen concentration was sampled. A 13th point was located at the mixer centerline. As a reference, the oxygen concentration of the inlet air was sampled as well. These experiments were performed with air and nitrogen as mixing gas but at conditions matching the velocity measured in water at the University of Twente (equal Reynolds numbers).

The measured concentration field is used to verify the calculations of the mixing performance by FLOW3D. There is however one problem. The mixing predicted by FLOW3D depends on a parameter, the Schmidt number: $Sc_t = \nu_t/D_t$. The turbulent diffusion coefficient D_t is not easily calculated from first principles and depends on the flow field. In the literature[1] values are mentioned of $Sc_t = 0.5$ for "free turbulence" and $Sc_t = 0.9$ for tube flow. If the T-junction indeed generates an improved mixing mechanism with respect to tube flow, then values of Sc_t less than 0.9 have to be expected.

The Schmidt number appropriate to the T-junction flow geometry was determined as follows. As a reference the situation was taken where the mixture ratio was 0.1 in the T-junction with a branch inlet diameter of 26 mm. The normalized deviation of the oxygen concentration from the cross-section average oxygen concentration $((y_i - y_{av})/y_{av})$ as measured in the seven sampling points is shown in *Figure 9a*. In view of the symmetry only half the tube cross-section is shown. For this case four simulations were performed with FLOW3D with different Schmidt numbers: 0.1, 0.2, 0.5, and 0.9. *Figure 9b* shows the calculated results in the mixer outlet, depicted is the normalized deviation of the oxygen concentration from the average, as in *Figure 9a*. Comparing the value at the center sample point in *Figure 9a* -7.42% with the values at various Schmidt numbers in *Figure 9b*, -3.74, -7.08, -14.4, and -20.8% ($Sc_t = 0.1$, 0.2, 0.5, 0.9) it can be concluded that $Sc_t = 0.2$ gives the best result. Also most of the other sample points in *Figure 9a* differ less in deviation from the average oxygen concentration than 30% with the calculated values in *Figure 9b* (with the exception of two points). On the basis of this result with the reference case (branch diameter 26 mm, flow ratio 0.1), it was decided that for this T-junction flow geometry a Schmidt number of 0.2 is appropriate. This decision has to be verified by simulations with $Sc = 0.2$ but with a different flow ratio and branch diameter. These have to compare with measurements as well.

Of all experiments and simulations, detailed information of the concentration distribution was available. In order to present this information efficiently, a parameter called the "mixture parameter" was calculated from the data at the 13 sampling points in the cross-section. This was defined as follows:

$$S_0 = \sqrt{\sum_{i=1}^{n} (y_i - y_{av})^2/(n-1)}$$

with y_i = mass fraction in point i, y_{av} = average mass fraction, and n = number of sampling points. In fact this is the spatial variance of the oxygen concentration. If the mixer performs well the oxygen concentration has minor spatial variance and the mixture parameter is small. *Table 1* shows the mixture parameter for the reference case (26 mm branch, flow ratio 0.1) for measurements and simulations with various Schmidt numbers. As above we see that a Schmidt number of about 0.2 gives the correct results.

Figure 10 shows the mixture parameter as a function of the inlet flow ratio for branch diameters of 10, 19, and 26 mm. The results for the measurements are indicated with filled markers and simulations (with $Sc_t = 0.2$) with open markers. From *Figure 10* it can be concluded that with the Schmidt number of 0.2 not only the reference case but also the other eight cases show a very good comparison of the

Table 1. Mixture parameter for branch inlet diameter 26 mm, mixture ratio 0.1.

Calculations with a Schmidt number (Sc) of	Mixture parameters: $S_0/\langle x \rangle^* 100$
0.1	4.76
0.2	6.36
0.5	9.61
0.9	12.63
Measurements	5.84

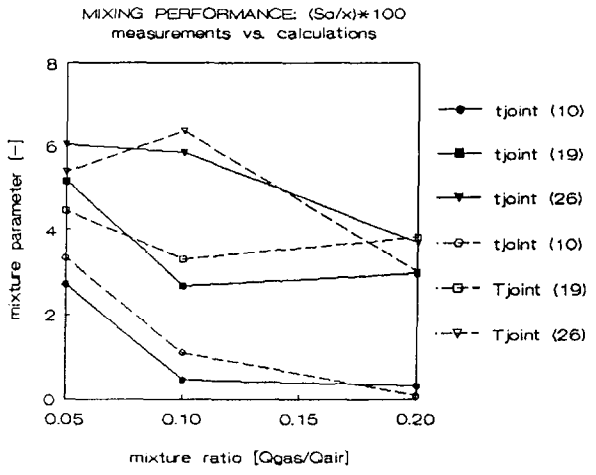

Figure 10. Mixture parameter as a function of mixture ratio for branch inlets of 10, 19, and 26 mm. Open symbols correspond to calculations; closed symbols correspond to measurements.

mixture parameter predicted by FLOW3D and the measured value. This indicates that for this type of flow geometry the choice was correct.

The general characteristic of the curves in *Figure 10* is that the mixture parameter decreases with an increasing mixture ratio. If the branch diameter is decreased the mixture parameter decreases as well. This hints at a dependence on the momentum of the jet coming from the branch. Below this will be analyzed with the help of the simulations.

The mixer pressure drop associated with the measurements in *Figure 10* increases quadratically with the mixture ratio. Also the improved mixing with a smaller branch diameter, as in *Figure 10*, has the disadvantage of an increased pressure drop. For example at a mixing ratio of 0.2, the mixer pressure drop is for branch diameter 26, 19, and 10 mm equal to 0.01, 0.06, and 0.09 mbar, respectively.[28]

This paper focuses on the T-junction with a 10, 19, or 26 mm diameter branch inlet. With respect to the fitting of the Schmidt number it is however interesting if $Sc_t = 0.2$ gives good results on the T-junction with 100 mm branch inlet as well. This because this mixer works in a range of very different momenta of the inlet flows. With FLOW3D version 3.1 and the mesh discussed in Section 4 the mixing was simulated in the 100 mm branch inlet mixer. The results for the mixture parameter at two mixture ratios are compared with measurements in *Table 2*. This shows that the mixture parameter is predicted with an error of less than 20% with a Schmidt number equal to 0.2. This is a very good result in view of the simplicity of the model and the limited accuracy of the measurements. The choice of

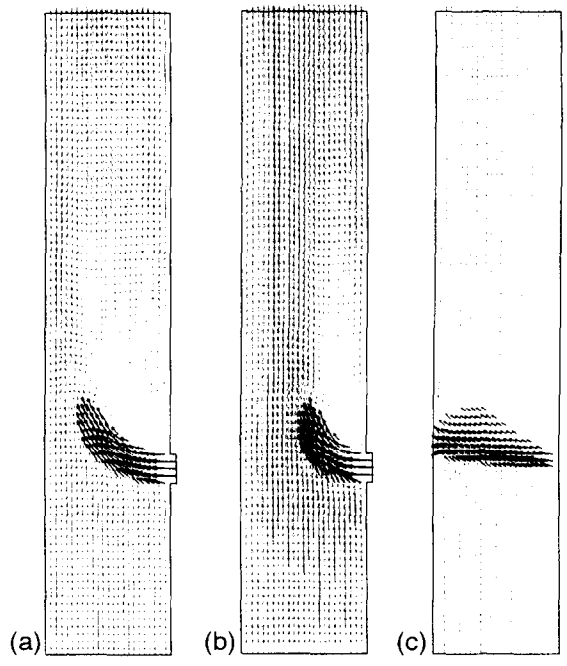

Figure 11. Vector plot of the velocity in the plane spanned by the centerlines of branch and main tube of the T-junction. (a) (Left) Mixture ratio = 0.2, branch diameter = 26 mm. (b) (Center) Mixture ratio = 0.1, branch diameter = 26 mm. (c) (Right) Mixture ratio = 0.1, branch diameter = 10 mm.

$Sc_t = 0.2$ for a T-junction flow seems to be correct since good results are obtained for a branch inlet varying from 10–100 mm and inlet flow ratios in the range 0.05–1.0.

7. Discussion

The results of the previous section give rise to the question what flow pattern leads to enhanced mixer performance in a T-junction. For an engineer designing a T-junction mixer not only the flow geometry but also the minimum mixer length is important to know. Another point is the amplitude of the temporal fluctuations of the oxygen concentration at the mixer outlet. In premixed combustion these temporal fluctuations can be as harmful for toxic emissions as spatial variance due to a mean concentration gradient. To measure these temporal fluctuations takes much more advanced experimental equipment than the relatively simple sample probe used here. Answers to these questions can be found with the help of the flow simulations with FLOW3D. As a reference the case with branch diameter 26 mm and flow ratio 0.1 is taken. From *Figure 10* we know that mixing here was poor (mixture parameter = 0.06). The associated flow pattern as calculated by

Table 2. Mixture parameter for branch inlet diameter 100 mm as a function of mixture ratio.

Mixture ratio	$S_0/\langle x\rangle^* 100$ (calculations)	$S_0/\langle x\rangle^* 100$ (measurements)
1	51.5	43.99
0.5	37.5	28.94

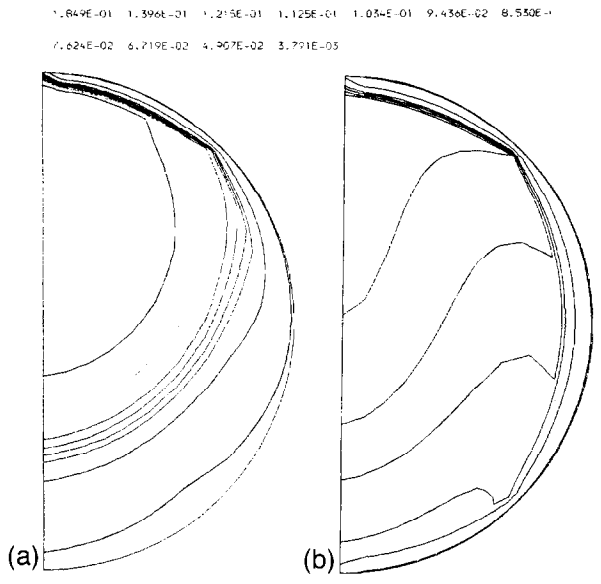

Figure 12. Iso concentration contours in the mixer outlet cross-section. (a) (Left) Mixture ratio = 0.1, branch inlet 26 mm, $Sc = 0.2$. (b) (Right) Mixture ratio = 0.1, branch inlet 10 mm, $Sc = 0.2$.

FLOW3D is depicted in *Figure 11b*. This is a vector plot of the velocity in the plane of symmetry spanned by the centerlines of the main tube and branch tube. The color indicates the magnitude of the radial velocity. *Figure 11b* shows that the branch inlet flow penetrates until the tube axis and is subsequently deflected. If the mixture ratio is increased (hence a larger branch flow) to 0.2 then the jet penetration increases (see *Figure 11a*) and the mixture parameter decreases to 0.03. Decreasing the branch inlet diameter to 10 mm at a mixture ratio of 0.1 leads to a jet penetrating to the opposite tube wall (*Figure 11c*) and a very low mixture parameter of 0.009. Hence for good mixing it is important to have a full jet penetration. This can be understood if we take a look at the average oxygen concentration field in the mixer outlet cross-section as calculated by FLOW3D.

Figure 12 shows contours of equal mass fraction of oxygen in one half of the (symmetric) mixer outlet cross-section. The pattern shows very clearly the degree of mixing of the nitrogen flow (downward initially) from the branch and the air flow. Since in *Figures* 12a and 12b identical contours were plotted, the actual values are less important for an evaluation. In *Figure 12a* the branch inlet diameter was 26 mm and the mixture ratio 0.1 (the reference case). This figure shows an oxygen concentration field with a large low oxygen concentration "bubble" in the upper part of the tube. Combining this with the associated velocity vector plot in *Figure 11b*, it can be concluded that this bubble contains gas from the deflected branch inlet jet. Apparently turbulent diffusion did not mix air into this jet. In *Figure 12b* the branch inlet was 10 mm and the mixture ratio 0.1. We see here a very well mixed concentration field with the iso oxygen fraction contours far apart. Hence the concentration gradients are small. Combining this with the associated velocity vector plot in *Figure 11c*, it can be concluded that, thanks to the good jet penetration, the nitrogen gas from the branch inlet is very well dispersed over the cross-section. A bubble recognizable as material from the branch is absent. Hence good mixing in a T-junction can be obtained by designing the branch inlet such that the branch inlet flow penetrates to the opposite tube wall. This disperses the jet flow and the material with it over the cross-section. Subsequently a mixer designer can decide what mixer length is necessary by examining cross-sections calculated at various axial distances. This way a good mixing small volume T-junction mixer can be designed.

A problem not discussed yet are the fluctuations of the oxygen concentration in the mixer outlet in time. Their amplitude was calculated for all cases by FLOW3D in the variable g. Above it was shown that in the 10 mm branch inlet, mixture ratio > 0.1, the spatial concentration fluctuations could be minimized. Does this apply to the temporal fluctuations as well? This is to be expected since the gradient of the average mass fraction is a factor in the source term of the g equation. This is verified in *Table 3*. This table shows in seven sample points the values calculated by FLOW3D for the reference case (26 mm branch inlet, mixture ratio 0.1) of the time-averaged mass fraction, the deviation of the spatial average, the variance of the temporal fluctuations, and their relative amplitude. Comparing the values in the third column with those in the fifth, it is seen that the spatial variance and the temporal fluctuations are of equal magnitude. This may, however, depend on the actual flow field and the nature of the turbulent fluctuations. Hence both spatial variance and temporal fluctuations have to be considered when designing a mixer. This is possible with the computational fluid dynamics package employed here thanks to the availability of the f, g equations in one of the combustion models. Unfortunately the predicted amplitude of the temporal fluctuations could not be verified in the present experimental set-up.

Table 3. Comparison of spatial and temporal concentration variations at branch inlet diameter 26 mm, mixture ratio 0.1, and calculated with $Sc = 0.2$.

	f_{local}	$(f-\tilde{f})/\tilde{f}$	g_{local}	$g^{1/2}/\tilde{f}$
1	0.123	0.34	5.19×10^{-4}	0.25
2	0.146	0.59	9.78×10^{-4}	0.34
3	0.159	0.73	1.01×10^{-3}	0.35
4	0.154	0.67	1.15×10^{-3}	0.37
5	0.136	0.48	1.43×10^{-3}	0.41
6	0.0702	−0.24	1.68×10^{-3}	0.45
7	0.00452	−0.95	6.79×10^{-5}	0.090

8. Conclusions

On the basis of the results presented in Sections 5 and 6 and the discussion in Section 7, several conclusions can be drawn. This will concern both the behavior of the mixing in the T-junction and the performance of the f, g equations in FLOW3D in predicting this behavior.

First of all it was shown that a T-junction can mix to an even concentration profile. Compared with other mixers[28] the pressure drop will be relatively high in a good mixing T-junction. Depending on the situation this can be a problem. The mixing performance is determined by the penetration of the branch inlet flow and hence depends on the mixing ratio of the flows. The best mixing is obtained when the branch inlet flow penetrates to the opposite tube wall.

In Section 5 it was shown that the flow field in the T-junction as predicted by FLOW3D with the k-ε turbulence model is in good agreement with the experiments. The choice of the turbulent Schmidt number for this jet in a cross-flow was discussed in Section 6. Here it was concluded that in order to have a good comparison of the mass transport predicted by FLOW3D and experiments in a T-junction, it is necessary to take a Schmidt number equal to 0.2.

The simulations indicate that temporal deviations of the average concentration can be expected to have a magnitude comparable with spatial concentration fluctuations. Hence it is important for good mixing to consider temporal as well as spatial concentration fluctuations. This is possible with FLOW3D using the mixed-burnt combustion model.

Acknowledgement

The authors gratefully acknowledge the financial support of N. V. Nederlandse Gasunie. They are indebted to Dr. R. Pieters for his assistance and the use of the experimental set-up at the laboratory of Gasunie Research. Dr. N. S. Wilkes, CFDS AEA, is acknowledged for his help in defining the calculational mesh of points in FLOW3D version 3.1 for a T-junction with a 100 mm diameter branch inlet tube.

Nomenclature

(x, y, z)	cartesian coordinates
ρ	fluid density
μ	the dynamic viscosity
P	the fluid pressure
k	the turbulent kinetic energy
ϵ	the dissipation of turbulent kinetic energy
ϕ	condensed variable
Γ_0	a diffusion coefficient
S_0	a source term
A, B	an inert species
Y_A	mass fraction
δ	the kronecker delta
Sc_t	the turbulent Schmidt number
μ_t	the turbulent dynamic viscosity
C_μ	fitting constant
φ_k, θ_ε, C_1, C_2	empirical constants
D_t	the turbulent diffusion coefficient
y_{av}	the average oxygen concentration
ν_t	the turbulent kinematic viscosity

References

1. Bird, R. B., Stewart, W. E., Lightfoot, E. N. *Transport Phenomena*, John Wiley & Sons, New York, 1960
2. Hinze, J. O. *Turbulence*, Mc Graw-Hill, 1972
3. Kuo, K. K. *Principles of Combustion*, John Wiley & Sons, New York, 1986
4. Launder, B. E. and Spalding, D. B. The numerical computation of turbulent flows, *Comp. Meth. Appl. Mech. Eng.*, 1974, **3**, 269–289
5. Patankar, S. V. *Numerical Heat Transfer and Fluid Flow*, Hemisphere Publ. Corp., New York, 1980
6. Mestayer, P. G. et al. Pollutant dispersion in the urban atmosphere: Simulation of turbulent flows using a k-ε model, *Ercoftac Bull.*, **16**, 1993, 22–28
7. Patankar, S. V., Basu, D. K., and Alpay, S. A. Prediction of the three-dimensional velocity field of a deflected turbulent jet, *J. Fluids Eng.*, 1977, **99**, 758
8. Spalding, D. B. Mathematische modelle turbulenter flammen, *VDI-Berichte*, 1970, **146**, 25–30
9. Wilkes, N. S., et al. The application of Harwell-FLOW3D to combustion problems, UK AEA Rept. AERE R 13508, 1989
10. Claus, R. W. Analytical calculation of a single jet in cross-flow and comparison with experiment, *Proceedings of the AIAA 21st Aerospace Sciences Meeting*, AIAA-83-0238, AIAA, New York, 1983
11. Claus, R. W. and Vanka, S. P. Multigrid calculations of a jet in crossflow, *J. Propulsion Power*, 1992, **8**(2), 425–431
12. Demuren, A. O. Modeling turbulent jets in crossflow, *Encyclopedia of Fluid Mechanics*, ed. N. P. Cheremisinoff), volume 2. Gulf Publ. Co., Houston, TX, 1985
13. Demuren, A. O. Characteristics of 3D turbulent jets in crossflow, Preprints for the *Symposium on Turbulence*, Univ. Missouri, Extension Division, Rolla, MO, 1990, pp. B1.1–B1.11
14. Demuren, A. O. Multigrid acceleration and turbulence models for computations of 3D turbulent jets in crossflow. *Int. J. Heat Mass Transfer* 1992, **35**(11), 2783–2794
15. Demuren, A. O. Characteristics of three-dimensional jets in crossflow, *Int. J. Eng. Sci.*, 1993, **31**(6), 899–913
16. Kim, S. and Benson, T. J. Calculation of a circular jet in crossflow with a multiple-time-scale turbulence model, *Int. J. Heat Mass Transfer*, 1992, **35(10)**, 2357–2365
17. Holdeman, J. D. 1993 Mixing of multiple jets with a confined subsonic crossflow, *Prog. Energy Combustion*, Sci. 1993, **19**(1), 31–70
18. Vranos, A. and Liscinsky, D. S. Planar imaging of jet mixing in crossflow, *AIAA J*, 1988, **26**(11), 1297–1298
19. Barata, J. M. M., Durao, D. F. G., and McGuirk, J. J. Numerical study of single impinging jets through a crossflow, *J. Aircraft* 1989, **26**(11), 1002–1008
20. Barata, J. M. M., Durao, D. F. G., Heitor, M. V., and McGuirk, J. J. Impingement of single and twin jets through a crossflow, *AIAA J.* 1991, **29**(4), 595–602
21. Jones, W. P. and McGuirk, J. J. Computations of a round turbulent jet discharging into a confined crossflow, *Turbulent Shear Flows*, ed. L. J. S. Bradbury, F. Durst, B. E. Launder, and F. W. Schmidt, Springer, New York, 1980
22. Crabb, D., Durao, D. F. G., and Whitelaw, J. H. A round jet normal to a crossflow, *J. Fluid Eng.* 1981, **103**, 142–152
23. Andreopoulos, J. and Rodi, W. Experimental investigation of jets in a crossflow, *J. Fluid Mech.* 1984, **138**, 93–127

24. Ferrell, G. B. and Lilley, D. G. Turbulence measurements of lateral jet injection into confined tubular crossflow, *AIAA / SAE / ASME / ASEE 21st Joint Propulsion Conference*, Monterey, CA, 1985, *AIAA-85-1102, AIAA*, New York, 1985
25. Horiuti, K. Assessment of two-equation models of turbulent passive scalar diffusion in channel flow, *J. Fluid Mech*, 1992, **238**, 405–433
26. Leboeuf, F., Huang, G. P., Kulisa, P., and Perrin, G. Model and computation of discrete jets in crossflow, *Eur. J. Mech.B / Fluids* 1991, **10**(6), 629–650
27. Rosendal, F. J. and Kok, J. B. W. Visualisation and LDA-measurements on swirling flows in expanding tubes, *Proceedings of the 4th International Conference on Laser Anemometry: Advances and Applications*, Cleveland, OH, 1991, ASME, New York, pp. 491–497
28. Van der Wal, S. Turbulent mixing of gases, Rep. University of Twente WB ThW TVM 93.001, Enschede, The Netherlands, 1993